Contract No:

This document was prepared in conjunction with work accomplished under Contract No. DE-AC09-08SR22470 with the U.S. Department of Energy.

Disclaimer:

Theoretical Study on the Interaction between Xenon and Positively Charged Silver Clusters in Gas Phase and on the (001) Chabazite Surface

Hoa G. Nguyen,[†] Gabor Konya,[†] Edward M. Eyring,[†] Douglas B. Hunter,[‡] and Thanh N. Truong*,[†]

Department of Chemistry, University of Utah, 315 South 1400 East, Salt Lake City, Utah 84112, and Savannah River National Laboratory, Aiken, South Carolina 29808

Received: March 27, 2009; Revised Manuscript Received: May 28, 2009

A systematic study on the adsorption of xenon on silver clusters in the gas phase and on the (001) surface of silver-exchanged chabazite is reported. Density functional theory at the B3LYP level with the cluster model was employed. The results indicate that the dominant part of the binding is the σ donation, which is the charge transfer from the 5p orbital of Xe to the 5s orbital of Ag and is not the previously suggested $d_\pi - d_\pi$ back-donation. A correlation between the binding energy and the degree of σ donation is found. Xenon was found to bind strongly to silver cluster cations and not to neutral ones. The binding strength decreases as the cluster size increases for both cases, clusters in the gas-phase and on the chabazite surface. The Ag^+ cation is the strongest binding site for xenon both in gas phase and on the chabazite surface with the binding energies of 73.9 and 14.5 kJ/mol, respectively. The results also suggest that the smaller silver clusters contribute to the negative chemical shifts observed in the ^{129}Xe NMR spectra in experiments.

1. Introduction

Although rare and expensive, xenon has a number of important applications in lighting, lasers, and the medical industries. In medicine, xenon is a promising general anesthetic,[1] while in the aerospace industry, it is a preferred fuel for the ion thruster in spacecrafts. Xenon has also been used as a research tool for ^{129}Xe NMR studies of zeolite structures and activity, particularly the location of acidic sites.[2] An excellent review on xenon's properties, application, and production can be found in the work of Häussinger et al.[3] Currently, xenon is produced by a costly process of fractional distillation of liquefied air. Given the increase in demand, alternative methods for producing xenon are of great interest. One recent study demonstrated the use of a polymer membrane to separate xenon from oxygen and nitrogen.[4] Zeolites, particularly silver-exchanged zeolites, are also being studied as promising materials for xenon separation.[5−8]

Xe was found to exhibit unusually strong interaction with silver-exchanged zeolites.[6−14] Furthermore, it is adsorbed more strongly in the silver-exchanged X and Y zeolites than in their sodium counterparts.[9−13] In Y zeolite, the initial isosteric heats of adsorption of xenon on Ag-exchanged and Na-exchanged materials were 31.0 and 18.5 kJ/mol, respectively.[14] Recently, experimental studies conducted by Munataka et al.,[6] Kuznicki et al.,[7] and us[8] have also shown that xenon can bind strongly to Ag-exchanged mordenite, ETS-10 (a type of titanosilicate), and chabazite, respectively. Although silver is necessary for zeolites to bind xenon, the nature of this unusually strong binding is still controversial.

Ionic silver was often thought to be the binding site for xenon on the basis of the observed trend in the strength of the interaction of xenon with oxidized > untreated > reduced AgX zeolites.[10] Both reduced AgX and untreated NaX are inert to xenon adsorption. However, in the study on Ag-ETS-10, Kuznicki et al. concluded that the strong binding with xenon is a result of its interaction with silver nanoparticles due to the lack of the yellow coloration generally associated with Ag^+ ions in molecular sieves.[7] This raises the question as to the nature of the binding site of Xe in Ag-exchanged zeolites, namely, silver exchanged ion sites inside zeolite or silver nanoclusters on the zeolite surface.

From the electronic configuration of Ag^+, $(4d)^{10}(5s)^0$, it was suggested that the large heat of adsorption of Xe on AgX and AgY zeolites is due to the $d_\pi - d_\pi$ back-donation, a charge transfer from the silver cation to xenon, from Ag^+ to Xe.[9−13] The $d_\pi - d_\pi$ back-donation is the electron donation from the 4d orbital of Ag^+ to the virtual 5d orbital of Xe. Such back-donation was also thought to be responsible for the unusual negative chemical shifts observed in the ^{129}Xe NMR in AgX and AgY zeolites.[9−13] However, a theoretical study by Freitag et al.[15] found that charge is transferred from Xe to Ag^+ with no indication of a 4d to 5d donation from Ag^+ to Xe. Furthermore, experimental and theoretical works on AgA zeolite of Moudrakovski et al.[16] and Jameson et al.[17] found only positive chemical shifts. They argued that Xe atoms are physisorbed in AgA zeolite rather than chemisorbed as in the work of Freitag et al. In their view, the negative chemical shifts in AgX and AgY zeolites remain a puzzle. Note that in such a discussion, these authors distinguished between physisorption and chemisorption by the adsorption distance and energy rather than by the nature of chemical bonding as well-accepted in surface science.

In the present work, we carried out a systematic theoretical study on the interaction of xenon with Ag^+ and small silver clusters in gas phase and adsorbed on chabazite surface. From our preliminary experimental data[8] and that of Kuznicki et al.,[18] the adsorption of xenon occurs on the surface of zeolite with ionic or metal silver nanoparticles serving as possible binding sites. The objective of this study was to provide a fundamental understanding of the nature of the interaction between Xe and Ag clusters on zeolite by determining: (1) the structural and electronic properties of the silver nanoparticles on the chabazite

[†] University of Utah.
[‡] Savannah River National Laboratory.

10.1021/jp902798w CCC: $40.75
Published on Web 06/25/2009

surface and (2) how these properties govern the affinity of Xe. Quantum chemistry calculations using cluster models were performed. The size of the Ag_n clusters was limited to four atoms in this study. The natural bond orbital (NBO) analysis[19] was used to study the electronic structures of the silver clusters. This method was previously used by Chen and Yang[20] to discover the d−π* back-donation between Ag-exchanged zeolite and O_2, N_2, and ethylene. In addition, interaction between Xe and a Na-exchanged chabazite system was also studied for comparison purposes.

2. Computational Details

For calculations involving free silver clusters in the gas phase, the optimized structures of these clusters from previous studies[21,22] were used as the starting points. For Xe−Ag−chabazite systems, cluster models were used to represent the binding sites of the zeolite materials. A cluster model of the zeolite binding site was made by cutting selected atoms surrounding the binding site from the crystal structure of chabazite taken from Database of Zeolite Structures.[23] The cluster models were treated quantum mechanically. More discussion on the accuracy of the cluster model and its application to zeolite systems can be found elsewhere.[24]

In the chabazite cage, the preferred site of Ag^+ is on top of the 6T ring.[25,26] Because Ag^+ is the seed for growing Ag clusters on zeolite, we assumed that the binding site for silver clusters is on the top of the 6T ring. The (001) surface was chosen for modeling because it is the only surface on which these 6T rings are fully exposed. Figure 1a shows three types of 6T rings on the (001) surface denoted R1, R2, and R3. In Figure 1b, calculated results indicated that a seed Ag^+ ion placed on R2 would sink deep inside the zeolite framework and that the framework would prevent additional silver atoms from binding to the seed Ag^+. For the R1 site (Figure 1c), the adsorbed Ag^+ is exposed above the surface and would be a good seed for other silver atoms to bind. The R3 site is similar to R1; however, the 4T and 8T rings surrounding it might hinder the agglomeration of silver atoms. For these reasons, we selected the R1 site for this study. At the R1 site, one tetrahedral site was selected to be the Brönsted acidic site and was substituted by one aluminum atom. To avoid edge effects in the cluster model, the 4T ring at the corner of the Al binding site was added. On the chabazite surface, tetrahedral Si atoms at the boundary were capped either with hydrogen atoms or OH groups as shown in Figure 1c. The capped atoms were fixed during geometry optimizations. The final $[Si_7AlO_{16}H_{14}]$ quantum cluster represents the best compromise between adequate structural representation of the R1 adsorption site for studying adsorption of metal clusters and computational demand for a reasonable number of quantum chemistry calculations. In the discussion below, [Cha] is used to denote $[Si_7AlO_{16}H_{14}]$. Therefore, Ag^+[Cha] means one Ag^+ on the R1 site of the (001) surface. In structural optimizations, atoms in the 6- and 4-member rings are allowed to move.

Second-order Møller−Plesset (MP2) perturbation theory calculation and nonlocal hybrid B3LYP density functional theory (DFT) were used in this study. The DFT/B3LYP level of calculation is well known for its consistency and reliability for studying interaction in zeolites. Since the focus of this study is on Xe−Ag_n^+ systems rather on neutral systems, the B3LYP method would be reasonably accurate despite some known inadequacies in describing dispersion interactions.[27,28] The 6-31G(d, p) basis set was used for the aluminum, silicon, hydrogen, and oxygen atoms in the 6T and 4T rings, and the

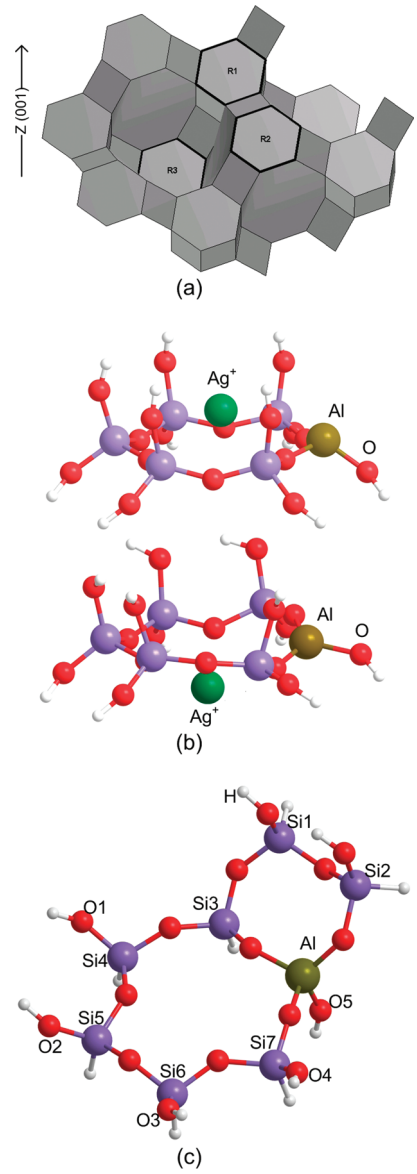

Figure 1. (a) Three types of 6T rings, R1, R2, and R3, on the (001) surface of the chabazite structure. (b) Starting (top structure) and optimized (bottom structure) geometries of a silver Ag^+ cation placed on the top of an R2 ring. (c) $[Si_7AlO_{16}H_{14}]$ cluster created by cutting the R1 site out of the chabazite surface.

LANL2DZ basis set with the effective core potential was used for the silver atom. Xenon was treated with the 3-21G(d) basis set. These basis sets of silver and xenon are sufficient since they yield the potential curve in agreement with those from the recent more accurate ab initio study of Yousef et al.[29] on smaller systems. To study the excited states of Xe−Ag^+, we employed the complete active space self-consistent field (CASSCF (2,4)) with the all electron relativistic basis set of Koga et al.[30,31] The counterpoise (CP) method[32,33] was applied to correct the basis set superposition error in the binding energies.

The cluster model ignores the effects of the extended zeolite framework on the adsorption properties mostly due to the Madelung potential from crystal atoms outside the cluster. A previous study on the adsorption of NO and CO on Cu-ZSM-5[34] found that such effects are small. One would also expect these effects to be small in Xe on the Ag_n^+[Cha] system. To confirm this, we have performed embedded cluster calculations for the Xe−Ag^+[Cha] system. To incorporate the environmental effects of the framework, we embedded the quantum cluster in

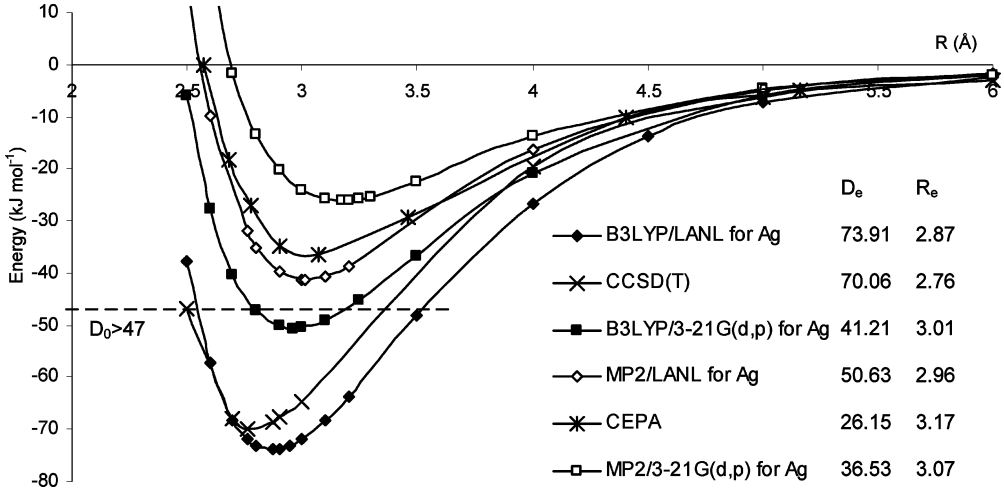

Figure 2. Potential energy curves for the gas phase Xe−Ag^+ compound calculated at different levels of theory. D_e (kJ/mol) and R_e (Å) are the potential depth and equilibrium distance, respectively. CCSD(T) and CEPA results are taken from ref 28 and ref 15, respectively.

a potential field of point charges. The surface charge representation of the electrostatic embedded potential (SCREEP) method[35] was used to construct these point charges. This methodology has been successfully employed in a number of zeolite systems.[34,36−39] B3LYP calculations for adsorption of Xe on the Ag_n^+ showed no major difference in the results from the cluster and embedded cluster models. Specifically, the difference in the calculated binding energies of Xe to Ag^+ on the chabazite surface using the embedded cluster and cluster models is 0.3 kJ/mol. Consequently, for simplicity we employed only the cluster model to represent the chabazite binding site in this study. All calculations were done using the Gaussian03 program.[40]

3. Results

3.1. Gas Phase. ***3.1.1. Xe−Ag$^+$.*** Studies on the binding between isolated monatomic Ag^+ and xenon can provide a reference point for studying the adsorption of Xe on the Ag_n^+[Cha] systems. The most accurate calculation to date for the Xe−Ag^+ potential curve was done by Yousef et al.[29] using the CCSD(T) level of theory with the quintuple-ζ basis set. The predicted binding energy of 70.1 kJ/mol is consistent with the established experimental lower limit of 47 kJ/mol.[41] The potential energy curves for Xe−Ag^+ from previous studies and our calculations are shown in Figure 2. Note that the present B3LYP calculations with the LANL basis set for Ag^+ yield D_e = 73.9 kJ/mol and R_e = 2.87 Å. This agrees well with D_e = 70.1 kJ/mol and R_e = 2.76 Å from CCSD(T) results from Yousef et al. The calculated MP2 binding energy of 50.1 kJ/mol is somewhat smaller but is still consistent with the established experimental lower limit of 47 kJ/mol. The agreement between the B3LYP results and those of CCSD(T) could be due to cancelation of errors in the DFT calculations, but it supports the choice of the B3LYP functional and the basis set used in this study.

NBO analysis can provide insight into the nature of the donor−acceptor interaction in the Xe−Ag^+ system. The electron occupancies of the important atomic orbitals, namely, the 5s, 4d, and 5p orbitals of Ag^+ and the 5p and 5d orbitals of Xe before and after adsorption, are listed in Table 1. Upon adsorption, 0.14 electron is transferred from Xe's 5p to the Ag^+ virtual 5s orbital. This is referred to as the σ donation due to the nature of the binding orbital of Xe−Ag^+ as shown in Figure 4.

The d_π−d_π back-donation suggested by Gedeon et al.[10] as a crucial factor for the Xe−Ag^+ interaction was not confirmed

TABLE 1: B3LYP/LANL NAO (Natural Atomic Orbital) Electron Occupancies of Gas Phase Ag^+ and Xe before and after Binding

Ag^+ + Xe	Ag^+_{before}	$(5s)^{0.0000}$	$(4d)^{10.0000}$	$(5p)^{0.0000}$
	Ag^+_{after}	$(5s)^{0.1373}$	$(4d)^{9.9920}$	$(5p)^{0.0115}$
	Ag^+_Δ[a]	**$(5s)^{0.1373}$**	**$(4d)^{-0.0080}$**	**$(5p)^{0.0115}$**
	Xe_{before}[b]	$(5p)^{6.0000}$	$(5d)^{0.0000}$	
	Xe_{after}[b]	$(5p)^{5.8535}$	$(5d)^{0.0065}$	
	Xe_Δ[a]	**$(5p)^{-0.1465}$**	**$(5d)^{0.0065}$**	
Na^+ + Xe	Na^+_{before}	$(3s)^{0.0000}$	$(3p)^{0.0000}$	
	Na^+_{after}	$(3s)^{0.0279}$	$(3p)^{0.0075}$	
	Na^+_Δ	**$(3s)^{0.0279}$**	**$(3p)^{0.0075}$**	
	Xe_Δ	**$(5p)^{-0.0414}$**	**$(5d)^{0.0040}$**	

[a] Δ indicates the differences in electron occupancies before and after binding. [b] The electronic configurations of Xe before binding are $(5p)^{6.0000}(5d)^{0.0000}$. Therefore, Xe_{before} and Xe_{after} are omitted in the following tables.

in this study. In Table 1, only 0.0080 electrons charge transfer out of the Ag^+'s 4d, and 0.0065 electrons are received by Xe's 5d orbitals. This indicates the magnitude of the d_π−d_π back-donation is insignificant. Compared to the σ donation, it is smaller by a factor of 1:18. We note that the magnitude of the d_π−d_π back-donation was found to be slightly larger for adsorption of N_2, O_2, or ethylene on Ag^+ in zeolite by Chen and Yang[20] but is also much smaller compared to the σ donation found here for the Xe−Ag^+[Cha] system. The present results indicate that the σ donation is the dominant factor governing the interaction of Xe with the Ag^+ cation in the ground state. This differs from previous suggestions on the role of the d_π−d_π back-donation for this system.[9−11]

Since the Ag^+ cation has several low-lying excited states, it is possible that the d_π−d_π back-donation is more noticeable in the excited state of Xe−Ag^+. To investigate such a possibility, CASSCF(2,4) calculations were carried out for several low-lying electronic states of the Xe−Ag^+ system. In particular, these include the ^{1}S ground state corresponding to the electronic configuration $(4d)^{10}$ of Ag^+, and the first and second excited states, ^{3}D and ^{1}D, respectively, corresponding to the Ag^+ configuration $(4d)^9(5s)^1$.

Figure 3 shows the potential energy curves for the three lowest electronic states of Xe−Ag^+. For Ag^+, CASSCF calculations yield the first and second excitation energies of 461.6 and 506.1 kJ/mol as compared to the experimental data of 467.8 and 550.4 kJ/mol.[42] The electronic configurations are listed in Table 2. Compared with the B3LYP results, the

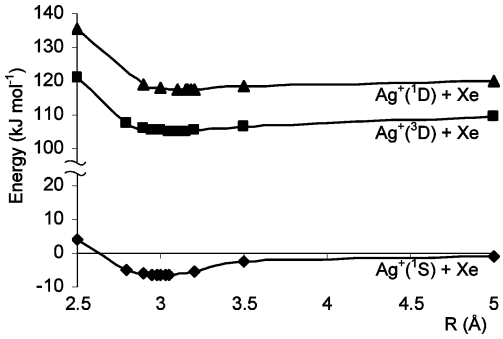

Figure 3. CASSCF potential energy curves for the ground state and the first two excited states of the Xe−Ag$^+$ compound.

TABLE 2: CASSCF NAO Electron Occupancies of Gas Phase Ag$^+$ and Xe before and after Binding

Ag$^+$(^{1}S) + Xe	Ag$^+_{\text{before}}$	(5s)$^{0.0000}$	(4d)$^{10.0000}$	(5p)$^{0.0000}$
	Ag$^+_{\text{after}}$	(5s)$^{0.0341}$	(4d)$^{9.9973}$	(5p)$^{0.0073}$
	Ag$^+_\Delta$	**(5s)$^{0.0341}$**	**(4d)$^{-0.0027}$**	**(5p)$^{0.0073}$**
	Xe$_\Delta$	**(5p)$^{-0.0578}$**	**(5d)$^{0.0145}$**	
Ag$^+$(^{3}D) + Xe	Ag$^+_{\text{before}}$	(5s)$^{1.0000}$	(4d)$^{9.0000}$	(5p)$^{0.0000}$
	Ag$^+_{\text{after}}$	(5s)$^{1.0256}$	(4d)$^{9.0304}$	(5p)$^{0.0181}$
	Ag$^+_\Delta$	**(5s)$^{0.0256}$**	**(4d)$^{0.0304}$**	**(5p)$^{0.0181}$**
	Xe$_\Delta$	**(5p)$^{-0.0888}$**	**(5d)$^{0.0096}$**	
Ag$^+$(^{1}D) + Xe	Ag$^+_{\text{before}}$	(5s)$^{1.0000}$	(4d)$^{9.0000}$	(5p)$^{0.0000}$
	Ag$^+_{\text{after}}$	(5s)$^{1.0198}$	(4d)$^{9.0271}$	(5p)$^{0.0171}$
	Ag$^+_\Delta$	**(5s)$^{0.0198}$**	**(4d)$^{0.0271}$**	**(5p)$^{0.0171}$**
	Xe$_\Delta$	**(5p)$^{-0.0798}$**	**(5d)$^{0.0090}$**	

TABLE 3: Binding Energy D_e (kJ/mol) and Equilibrium Distance R_e (Å) of Xe Adsorption on Gas Phase Ag$_n^+$ Clusters and Na$^+$ Cation[a]

	D_e	R_e
Ag$_1^+$	73.9	2.87
Ag$_2^+$	42.6	2.97
Ag$_3^+$	33.3	3.02
Ag$_4^+$	27.6	3.06
Na$^+$	46.1	3.04

[a] B3LYP/LANL for Ag, with CP correction.

CASSCF calculations predict smaller magnitudes of both the σ donation and the $d_\pi-d_\pi$ back-donation for the ground state. The difference between the excited states and the ground state is the promotion of one electron from 4d to 5s in Ag$^+$. This reduces the amount of electron that can be transferred to Ag$^+$'s 5s in the excited states. The charge transfers to the Ag$^+$'s 5s for the ground state, first, and second excited states are 0.0341, 0.0256, and 0.0198 electron, respectively. In the excited states, because Ag$^+$'s 4d orbital has only 9 electrons, this orbital can receive an electron from Xe's 5p upon binding. The occupancy change in Ag's 4d is −0.0027, 0.0304, and 0.0271 electrons for the ground state, ^{3}D, and ^{1}D excited states, respectively. For the $d_\pi-d_\pi$ back-donation, the 4d orbital of silver is the electron acceptor, thus only small $d_\pi-d_\pi$ back-donation is found in the ground state but none in the excited states of the Xe−Ag$^+$ system.

3.1.2. Xe−Na$^+$. For comparison, the binding energy between Xe and Na$^+$ was also calculated and has a magnitude of 46.1 kJ/mol (Table 3) as compared to 73.9 kJ/mol for Xe−Ag$^+$. The charge transferred to Na$^+$'s 3s from Xe's 5p is 0.028 electrons as compared to 0.14 electrons in the Xe−Ag$^+$ system. It is known that the degree of electron transfer is proportional to the overlap between the donor and acceptor orbitals. Since Na$^+$'s 3s orbtial is much smaller than the Ag$^+$'s 5s orbital, which is comparable in size to Xe's 5p orbital, one can expect smaller overlap between the Na$^+$'s 3s orbital and Xe's 5p orbital and thus a smaller amount of electron transfer.

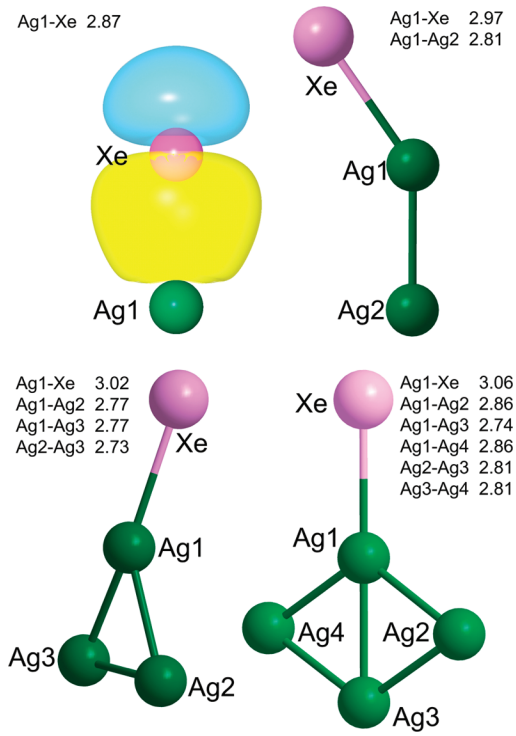

Figure 4. Xenon binds to gas phase Ag$_n^+$ clusters. σ donation bonding orbital of Xe and Ag$^+$ is generated using NBOView.[19] Distances (Å) between silver and xenon atoms are shown.

TABLE 4: B3LYP/LANL NAO Electron Occupancies of the Gas Phase Ag$_{2,3,4}^+$ Clusters and Xe before and after Binding

Ag$_2^+$ + Xe	Ag1$_{\text{before}}$	(5s)$^{0.4983}$	(4d)$^{9.9851}$	(5p)$^{0.0165}$
	Ag1$_{\text{after}}$	(5s)$^{0.5593}$	(4d)$^{9.9816}$	(5p)$^{0.0169}$
	Ag1$_\Delta$	**(5s)$^{0.0536}$**	**(4d)$^{-0.0034}$**	**(5p)$^{0.0004}$**
	Ag$_2^+{}_{\text{before}}$	(5s)$^{0.9967}$	(4d)$^{19.9701}$	(5p)$^{0.0329}$
	Ag$_2^+{}_{\text{after}}$	(5s)$^{1.1113}$	(4d)$^{19.9639}$	(5p)$^{0.0456}$
	Ag$_2^+{}_\Delta$	**(5s)$^{0.1146}$**	**(4d)$^{-0.0063}$**	**(5p)$^{0.0127}$**
	Xe$_\Delta$	**(5p)$^{-0.1167}$**	**(5d)$^{0.0034}$**	
Ag$_3^+$ + Xe	Ag1$_{\text{before}}$	(5s)$^{0.6689}$	(4d)$^{9.9773}$	(5p)$^{0.0201}$
	Ag1$_{\text{after}}$	(5s)$^{0.7190}$	(4d)$^{9.9697}$	(5p)$^{0.0281}$
	Ag1$_\Delta$	**(5s)$^{0.0501}$**	**(4d)$^{-0.0077}$**	**(5p)$^{0.0080}$**
	Ag$_3^+{}_{\text{before}}$	(5s)$^{2.0070}$	(4d)$^{29.9320}$	(5p)$^{0.0529}$
	Ag$_3^+{}_{\text{after}}$	(5s)$^{2.1199}$	(4d)$^{29.9232}$	(5p)$^{0.0681}$
	Ag$_3^+{}_\Delta$	**(5s)$^{0.1130}$**	**(4d)$^{-0.0088}$**	**(5p)$^{0.0078}$**
	Xe$_\Delta$	**(5p)$^{-0.1044}$**	**(5d)$^{0.0029}$**	
Ag$_4^+$ + Xe	Ag1$_{\text{before}}$	(5s)$^{0.7289}$	(4d)$^{9.9712}$	(5p)$^{0.0419}$
	Ag1$_{\text{after}}$	(5s)$^{0.7848}$	(4d)$^{9.9687}$	(5p)$^{0.0422}$
	Ag1$_\Delta$	**(5s)$^{0.0559}$**	**(4d)$^{-0.0024}$**	**(5p)$^{0.0003}$**
	Ag$_4^+{}_{\text{before}}$	(5s)$^{2.9904}$	(4d)$^{39.8968}$	(5p)$^{0.1075}$
	Ag$_4^+{}_{\text{after}}$	(5s)$^{3.0951}$	(4d)$^{39.8914}$	(5p)$^{0.1128}$
	Ag$_4^+{}_\Delta$	**(5s)$^{0.1048}$**	**(4d)$^{-0.0054}$**	**(5p)$^{0.0054}$**
	Xe$_\Delta$	**(5p)$^{-0.0967}$**	**(5d)$^{0.0026}$**	

3.1.3. Xe−Ag$_{2,3,4}^+$. The optimized structures of Xe adsorbed on Ag$_{2,3,4}^+$ clusters are shown in Figure 4. The binding energies between xenon and the silver cation clusters are given in Table 3. The electronic configurations of the silver atoms that bind directly to xenon indicated as Ag1 in Figure 4 are listed in Table 4. The total electronic configuration for the silver cluster is defined as the summation of the electron occupancies of all of the atoms in the silver cluster and is also reported. For Xe, only the differences in the Xe electron occupancy upon adsorption are shown.

Increasing the cluster size from monatomic Ag$^+$ to Ag$_4^+$, the equilibrium distance R_e increases from 2.87 to 3.06 Å, while

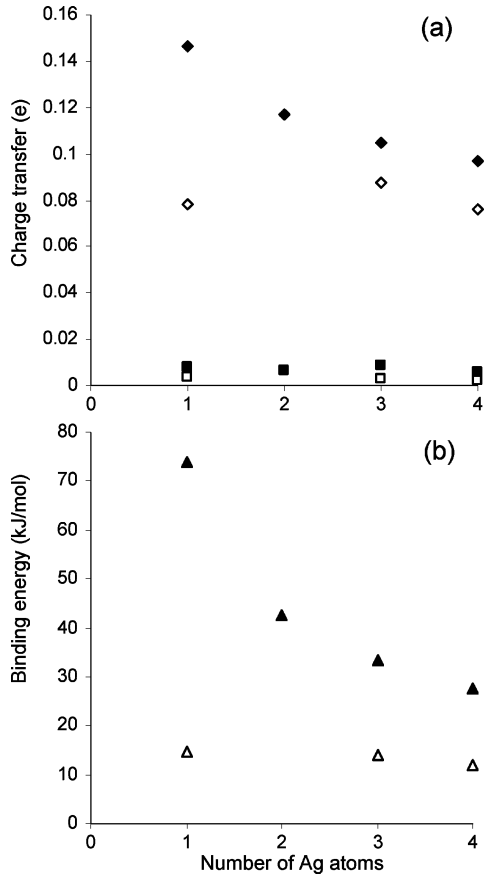

Figure 5. (a) Magnitude of the σ donation (◆, ◇) and the $d_\pi - d_\pi$ back-donation (■, □). (b) Binding energies of xenon and ionic silver clusters (▲, △). Filled markers are for the gas phase silver clusters; unfilled markers are for silver clusters on the (001) chabazite surface.

the binding energy decreases from 73.9 to 27.6 kJ/mol, and the σ donation decreases from 0.1470 to 0.0970 electrons received by the silver cluster. Similar to the $Xe-Ag^+$ system, the $d_\pi - d_\pi$ back-donation can be extended as the total loss of electrons in the 4d orbital in all silver atoms of the cluster. NBO analysis shows that the $d_\pi - d_\pi$ back-donation is negligible compared with the σ donation. For instance, for the $Xe-Ag_2^+$ compound, the magnitudes of electron transfer in the σ donation and the $d_\pi - d_\pi$ back-donation are 0.117 and 0.006 electrons, respectively. The correlations between the cluster sizes, the electron transfers, and the binding energies are shown in Figure 5.

The decrease in the binding energy of Xe as the Ag_n^+ cluster size increases is due to the charge delocalization effect. The +1 charge is distributed over all silver atoms of the cluster. Consequently, the electron occupancy in the Ag 5s orbitals increases with cluster size. Such higher electron occupancy in the Ag 5s orbital hinders electron transfer from the Xe 5p orbital to these orbitals. Consequently, as the cluster size increases, a smaller number of electrons is transferred from Xe to the silver cluster, leading to weaker binding energy.

3.2. Chabazite Surface. ***3.2.1. $Ag_{1,3,4}^+$ Clusters on the (001) Chabazite Surface.*** The structures of silver cluster cations on the 6T ring of the (001) chabazite surface were optimized with the seed of a Ag^+ at the center of the ring. Silver clusters with 1, 3, and 4 Ag atoms were found to be stable, whereas dimer Ag_2^+ was not stable at this adsorption site. Unlike the isolated Ag_4^+ cluster, Ag_4^+ on the chabazite surface has a tetrahedral configuration instead of a planar one. Upon binding with xenon, all of the silver cluster structures remain nearly the same. We

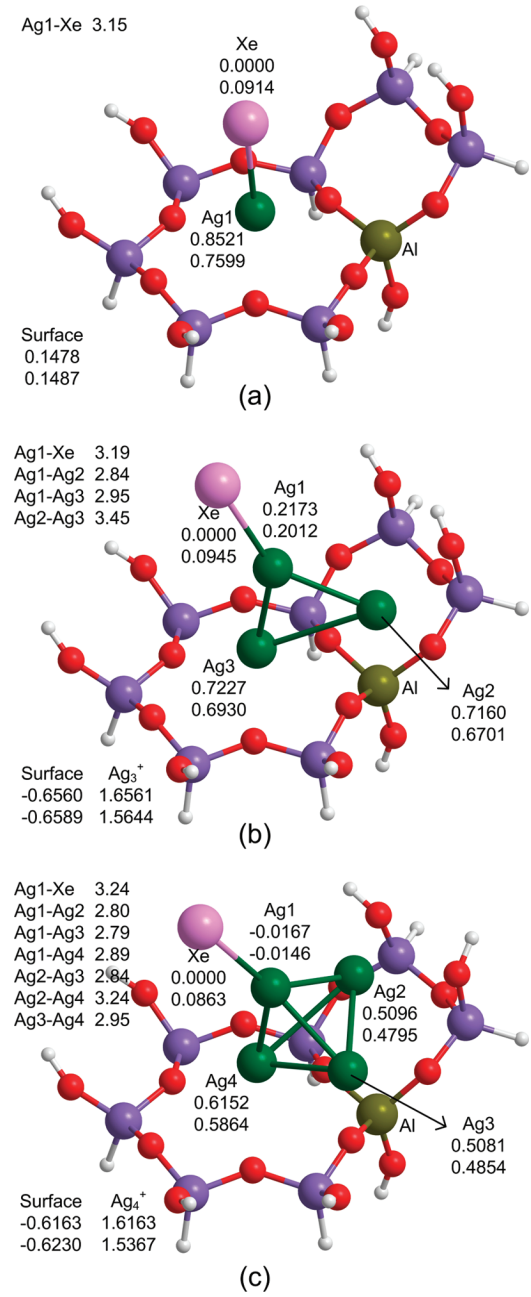

Figure 6. Optimized structures of xenon adsorption on ionic $Ag_{1,3,4}$ clusters on the chabazite surface. Natural charges obtained from NBO analysis are showed under selected atoms. The top number is before binding, and the bottom one is after binding. The charge of the $[Si_7AlO_{16}H_{14}]$ quantum cluster is considered as the surface charge. Distances (Å) between selected silver atoms and xenon atom are shown.

found that adsorption of Xe has an insignificant effect on the structures of the adsorbed silver clusters. For simplicity, only the optimized structures of the silver clusters with xenon are shown in Figure 6.

The charges of silver atoms in Figure 6 reveal the electronic effect of the chabazite surface on the adsorbed silver clusters. The total charges of silver clusters and the surface are also given. The surface charge is the charge of the $[Si_7AlO_{16}H_{14}]$ quantum cluster. We found that there are dramatic differences in the electronic structures of Ag^+[Cha] as compared to those of Ag_3^+[Cha] and Ag_4^+[Cha]. In particular, for the Ag^+[Cha] system, 0.1478 electrons are transferred from [Cha] to Ag^+, making Ag^+ less positive than its original +1 charge. There is

TABLE 5: Binding Energy D_e (kJ/mol) and Equilibrium Distance R_e (Å) of Xe Adsorption on $Ag_{1,3,4}^+$ Clusters on the (001) Chabazite Surface

	D_e	R_e
Ag_1^+	14.5	3.15
Ag_3^+	14.1	3.19
Ag_4^+	11.8	3.24

TABLE 6: B3LYP/LANL NAO Electron Occupancies of $Ag_{1,3,4}^+$ Clusters on the (001) Chabazite Surface and of Xe before and after Binding

$Ag^+ + Xe$	$Ag1_{before}$	$(5s)^{0.1581}$	$(4d)^{9.9531}$	$(5p)^{0.0240}$
	$Ag1_{after}$	$(5s)^{0.2251}$	$(4d)^{9.9663}$	$(5p)^{0.0310}$
	$Ag1_{\Delta}$	**$(5s)^{0.0670}$**	**$(4d)^{0.0132}$**	**$(5p)^{0.0070}$**
	Xe_{Δ}	**$(5p)^{-0.0784}$**	**$(5d)^{0.0033}$**	
$Ag_3^+ + Xe$	$Ag1_{before}$	$(5s)^{0.7737}$	$(4d)^{9.9849}$	$(5p)^{0.0063}$
	$Ag1_{after}$	$(5s)^{0.7800}$	$(4d)^{9.9810}$	$(5p)^{0.0095}$
	$Ag1_{\Delta}$	**$(5s)^{0.0062}$**	**$(4d)^{-0.0039}$**	**$(5p)^{0.0032}$**
	$Ag_3^+{}_{before}$	$(5s)^{1.3500}$	$(4d)^{29.8797}$	$(5p)^{0.0874}$
	$Ag_3^+{}_{after}$	$(5s)^{1.4298}$	$(4d)^{29.8743}$	$(5p)^{0.1040}$
	$Ag_3^+{}_{\Delta}$	**$(5s)^{0.0799}$**	**$(4d)^{-0.0053}$**	**$(5p)^{0.0166}$**
	Xe_{Δ}	**$(5p)^{-0.0878}$**	**$(5d)^{0.0026}$**	
$Ag_4^+ + Xe$	$Ag1_{before}$	$(5s)^{0.9831}$	$(4d)^{9.9731}$	$(5p)^{0.0607}$
	$Ag1_{after}$	$(5s)^{0.9829}$	$(4d)^{9.9696}$	$(5p)^{0.0580}$
	$Ag1_{\Delta}$	**$(5s)^{-0.0002}$**	**$(4d)^{-0.0024}$**	**$(5p)^{-0.0027}$**
	$Ag_4^+{}_{before}$	$(5s)^{2.3120}$	$(4d)^{39.8566}$	$(5p)^{0.1773}$
	$Ag_4^+{}_{after}$	$(5s)^{2.3859}$	$(4d)^{39.8518}$	$(5p)^{0.1854}$
	$Ag_4^+{}_{\Delta}$	**$(5s)^{0.0739}$**	**$(4d)^{-0.0048}$**	**$(5p)^{0.0080}$**
	Xe_{Δ}	**$(5p)^{-0.0762}$**	**$(5d)^{0.0022}$**	

a total of 0.1581 electrons in the 5s orbital of Ag^+ as listed in Table 5. In contrast to the Ag^+[Cha] system, Ag_3^+ and Ag_4^+ transfer more than 0.6 electrons to the zeolite surface upon adsorption, becoming more positive, specifically 1.6561 and 1.6163, respectively. This is because the additional Ag atoms are close to the O atoms of the 6T ring, which have higher electron affinity than Ag. Consequently, Ag_3^+ and Ag_4^+ on the surface have fewer electrons in the 5s orbitals compared with that of their gas phase counterparts. For instance, the total number of electrons in the 5s orbitals of Ag_3^+ in the gas phase and on the zeolite surface is 2.0070 and 1.3500 electrons, respectively. This suggests that such differences may lead to very different binding energies for Xe on Ag^+ and on larger clusters on the chabazite surface.

3.2.2. Xenon Binding with $Ag_{1,3,4}^+$ Clusters on the (001) Chabazite Surface. The cation silver clusters on the chabazite surface lose part of their affinity for xenon compared to that of their isolated counterparts. Results of binding energies are shown in Figure 5 and Table 5. The binding energy D_e declines, and the equilibrium distance R_e increases when the cluster size increases. Analysis of natural atomic orbital occupancies in Table 6 provides insight into this loss of Xe affinity. The appearance of 0.0158 electrons in the Ag's 5s orbital in the Xe−Ag^+[Cha] system causes a reduction in the charge transfer from 0.146 in isolated Xe−Ag^+ to 0.0670 electrons. The binding energy decreases significantly from 73.9 to 14.5 kJ/mol.

There are large gaps in the binding energies of Xe with Ag^+ and $Ag_{3,4}^+$ in the gas phase. However, on the chabazite surface, the binding energies are much closer and are 14.5, 14.1, and 11.8 kJ/mol, respectively. The results are in fact counterintuitive with the calculated total charges of the adsorbed Ag clusters mentioned above. The larger positive charge on the adsorbed $Ag_{3,4}^+$ clusters indicates the larger degree of vacancy in their 5s orbitals. From the above discussion, this would suggest the larger degree of σ donation and thus larger binding energy. The results confirm that the σ donation of Xe on the adsorbed Ag^+ is smaller than that of the adsorbed Ag_3^+ (0.0784 < 0.0878). Closer examination reveals that the binding energy of the Xe to Ag_n^+ cluster depends more closely on the occupancy of the Ag1 atom that binds directly with Xe rather than the total charge of the cluster and the degree of charge transfer from Xe to that atom upon adsorption. Unlike Ag1 in the isolated $Ag_{3,4}^+$ clusters, which receive almost half of the σ donation, Ag1 in the adsorbed Ag_3^+[Cha] receives only 8% of the total charge transfer from Xe upon adsorption. In Ag_4^+[Cha], the charge of Ag1 is almost unchanged after binding with Xe (from −0.0167 to −0.0146 in Figure 6). A large part of the charge transfer from Xe resides on other silver atoms that bind directly to the zeolite surface. In $Ag_{3,4}^+$ clusters in Figure 6, the changes in charge of silver atoms other than Ag1 are more significant than that of Ag1. Consequently, the small changes in the Ag1 charge upon adsorption provide an explanation for the small differences in the Xe binding energies for different clusters.

3.2.3. Xenon Binding with Neutral $Ag_{1,3,4}$ and Na^+ Clusters on the (001) Chabazite Surface. For completeness, the interaction of xenon with reduced silver clusters on the chabazite surface was also studied. No binding with xenon was found on any size of neutral silver clusters. The inert behavior of reduced Ag-chabazite is in agreement with previous experimental observations.[10]

Adsorption of Xe on the Na^+[Cha] was also studied for comparison with Xe on Ag^+[Cha]. The calculated binding energy of Xe on Na^+[Cha] is 7.2 kJ/mol, which is smaller than that of Ag^+[Cha] because of the difference in size between 3s and 5s orbitals. This value is also smaller than that of free Na^+. Without the charge transfer from chabazite, the 3s orbital of isolated Na^+ is more susceptible to electron transfer from Xe's 5p orbital.

Finally, all of the silver clusters in our study, free or bound to the chabazite surface, follow a pattern: increase in the cluster size leads to diminishing xenon binding strength. In the isolated clusters, Ag^+ is the most attractive. On the chabazite surface, Ag^+ has slightly larger Xe binding affinity compared to that of larger clusters. It is possible to extrapolate this trend to bigger nanoparticles found in the experiments.[7,8]

4. Discussion

4.1. Correlation between σ Donation and Xe Binding Properties. Traditionally, interaction between Xe and Ag_n^+ can be described by the attractive charge-induced polarization and the van der Waals repulsion. Bellert and Breckenridge[43] introduced a model potential for monatomic cations and noble gases consisting of attractive terms with dependence on distance R ranging from $1/R^4$ to $1/R^8$ and an Ae^{-bR} repulsive term. Unfortunately, these potential functions rely on point charges and thus are not readily applicable for clusters where charge delocalization occurs. To provide further insight into interaction between Xe on adsorbed Ag_n^+ on the chabazite surface, the correlations between the binding energy with the equilibrium Xe−Ag bond distance with the σ donation are plotted in Figures 7 and 8, respectively. Note that the binding energy correlates well with the binding distance and the degree of σ donation. As the binding distance decreases, the overlap between the Ag's 5s and Xe's 5p orbitals increases, leading to larger σ donation and consequently larger binding energy. The present study found that the zeolite framework can greatly reduce the Xe binding capability of Ag_n^+ clusters.

4.2. Chemical Shift. In this study, the d_π−d_π back-donation is negligible and therefore cannot be used to explain the unusual negative shifts in the ^{129}Xe NMR experiments on AgX and AgY zeolites. These shifts were first explained by

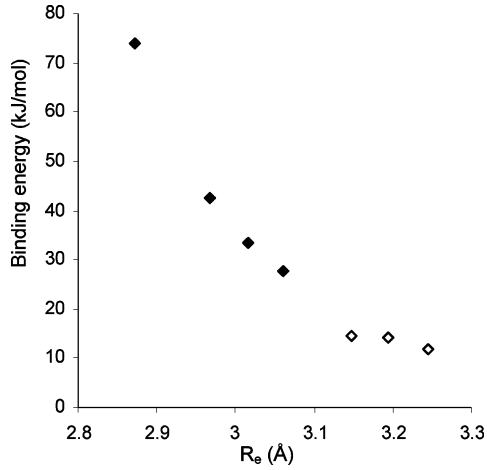

Figure 7. Binding energy of the $Xe-Ag_n^+$ system vs the magnitude of the σ donation. Filled markers are for gas phase silver clusters; unfilled markers are for silver clusters on the (001) chabazite surface.

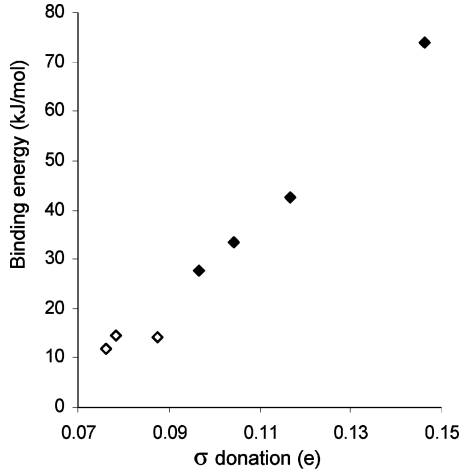

Figure 8. Binding energy of the $Xe-Ag_n^+$ system versus the equilibrium distance. Filled markers are for gas phase silver clusters; unfilled markers are for silver clusters on the (001) chabazite surface.

the shielding effect formed by the $d_\pi-d_\pi$ back-donation from Ag^+'s 4d orbital to Xe's 5d orbital by Gedeon et al.[10] However, ab initio calculations on gas phase Ag^+ and Xe by Freitag et al.[15] indicated that the shielding effect is attributed to the mixing between the 5p, 4p, and 3p orbitals of Xe with the 4d orbitals of Ag^+. In Freitag et al.'s study, the ^{129}Xe NMR chemical shift curve for $Xe-Ag^+$ shows two regions: (1) positive shift due to the deshielding polarization of the Xe charge distribution by Ag^+ when the $Xe-Ag^+$ distance is greater than 3.7 Å and (2) negative shift due to the exponentially increasing shielding contributions of the p orbitals at Xe by mixing with Ag^+'s d orbitals when the $Xe-Ag^+$ distance is smaller than 3.7 Å. Using Mulliken analysis, Freitag et al. did not find any $d_\pi-d_\pi$ back-donation but found instead the electron transfer from the p orbitals of Xe to the s and p orbitals of Ag^+. Results of Freitag et al. were later confirmed by the works of Moudrakovski et al. and Jameson et al. on AgA zeolite.[16,17] According to these authors, a larger fraction of Xe atoms in AgA has $Xe-Ag^+$ distances greater than 3.7 Å, giving positive chemical shift. This could easily overwhelm the negative contributions from less than 3.7 Å configurations.

According to our calculations, for small ionic silver clusters in the gas phase and on the (001) chabazite surface, the σ donation is far more dominant than the $d_\pi-d_\pi$ back-donation, resulting in a total charge transfer from xenon to silver. Our results of the Xe binding distances in Table 5 are less than 3.7 Å and thus suggest that the observed negative NMR shift are due to adsorption of Xe on small Ag_n^+ clusters.

5. Summary

We presented a computational study of the adsorption of xenon on silver clusters ($n = 1-4$ atoms) in the gas phase and on the chabazite surface using cluster models. The binding between xenon and silver, in essence, is the σ donation, which is the charge transfer from the 5p orbital of xenon to the 5s orbital of silver. Our results prove that Ag_{1-4} clusters have enhanced affinity for xenon but only in the ionic state because of the empty Ag's 5s orbitals. When reduced to neutral, these silver clusters show no Xe affinity. Increasing the size of cation clusters in our computational model weakens xenon adsorption because of the delocalization of the positive charge. The ionic gas phase silver clusters bind xenon much more strongly than those adsorbed on the chabazite surface. We found a strong correlation between the binding energy and the σ donation. The results indicate that the $d_\pi-d_\pi$ back-donation plays an insignificant role in Xe binding. Using the binding distance as an argument for physisorption or chemisorption, our results suggest that the observed negative NMR chemical shift is from Xe adsorption on small Ag_n^+ clusters.

Acknowledgment. This document was prepared in conjunction with work accomplished under Contract No. DE-AC09-08SR22470 with the U.S. Department of Energy. All calculations were performed at the Center for High Performance Computing at the University of Utah. H.G.N. thanks the Vietnam Education Foundation for their partial support and Dr. Treesukol for his advice.

References and Notes

(1) Goto, T. *Can. J. Anesth.* **2002**, *49*, 335.
(2) Ito, T.; Fraissard, J. *J. Chem. Phys.* **1982**, *76*, 5225.
(3) Häussinger, P.; Glatthaar, R.; Rhode, W.; Kick, H.; Benkmann, C.; Weber, J. Noble Gases. In *Ullmann's Encyclopedia of Industrial Chemistry*; Wiley: New York, 2001.
(4) Jeanes, T. O.; Jensvold, J. A. Vol. U.S. Patent 6168649, 2001.
(5) Barrer, R. M.; Papadopoulos, R. *Proc. R. Soc. A* **1972**, *326*, 315.
(6) Munakata, K.; Kanjo, S.; Yamatsuki, S.; Koga, A.; Ianovski, D. *J. Nucl. Sci. Technol.* **2003**, *40*, 695.
(7) Kuznicki, S. M.; Anson, A.; Koenig, A.; Kuznicki, T. M.; Haastrup, T.; Eyring, E. M.; Hunter, D. *J. Phys. Chem. C* **2007**, *111*, 1560.
(8) Konya, G.; Eyring, E. M.; Hunter, D., unpublished work.
(9) Fraissard, J.; Gedeon, A.; Chen, Q.; Ito, T. *Stud. Surf. Sci. Catal.* **1991**, *69*, 461.
(10) Gedeon, A.; Burmeister, R.; Grosse, R.; Boddenberg, B.; Fraissard, J. *Chem. Phys. Lett.* **1991**, *179*, 191.
(11) Grosse, R.; Burmeister, R.; Boddenberg, B.; Gedeon, A.; Fraissard, J. *J. Phys. Chem.* **1991**, *95*, 2443.
(12) Grosse, R.; Gedeon, A.; Watermann, J.; Fraissard, J.; Boddenberg, B. *Zeolites* **1992**, *12*, 909.
(13) Gedeon, A.; Fraissard, J. *Chem. Phys. Lett.* **1994**, *219*, 440.
(14) Watermann, J.; Boddenberg, B. *Zeolites* **1993**, *13*, 247.
(15) Freitag, A.; van Wüllen, C.; Staemmler, V. *Chem. Phys.* **1995**, *192*, 267.
(16) Moudrakovski, I. L.; Ratcliffe, C. I.; Ripmeester, J. A. *J. Am. Chem. Soc.* **1998**, *120*, 3123.
(17) Jameson, C. J.; Lim, H.-M. *J. Chem. Phys.* **1997**, *107*, 4373.
(18) Kuznicki, S. M.; Kelly, D. J. A.; Bian, J.; Lin, C. C. H.; Liu, Y.; Chen, J.; Mitlin, D.; Xu, Z. *Microporous Mesoporous Mater.* **2007**, *103*, 309.
(19) Glendening, E. D.; Badenhoop, J. K.; Reed, A. E.; Carpenter, J. E.; Bohmann, J. A.; Morales, C. M.; Weinhold, F. *NBO 5.0*, 2001.
(20) Chen, N.; Yang, R. T. *Ind. Eng. Chem. Res.* **1996**, *35*, 4020.
(21) Huda, M. N.; Ray, A. K. *Eur. Phys. J.* **2003**, *22*, 217.
(22) Wang, Y.; Gong, X. G. *Eur. Phys. J.* **2005**, *34*, 19.

(23) Baerlocher, C.; McCusker, L. B. Database of Zeolite Structures. www.iza-structure.org/databases.

(24) Hill, J.; Subramanian, L.; Maiti, A. *Molecular Modeling Techniques in Material Sciences*; Taylor & Francis: Oxford, U.K., 2005.

(25) Calligaris, M.; Mezzetti, A.; Nardin, G.; Randaccio, L. *Zeolites* **1984**, *4*, 323.

(26) Calligaris, M.; Nardin, G.; Randaccio, L. *Zeolites* **1983**, *3*, 205.

(27) Johnson, E. R.; Wolkow, R. A.; DiLabio, G. A. *Chem. Phys. Lett.* **2004**, *394*, 334.

(28) Pérez-Jordá, J. M.; Becke, A. D. *Chem. Phys. Lett.* **1995**, *233*, 134137.

(29) Yousef, A.; Shrestha, S.; Viehland, L. A.; Lee, E. P. F.; Gray, B. R.; Ayles, V. L.; Wright, T. G.; Breckenridge, W. H. *J. Chem. Phys.* **2007**, *127*, 154309.

(30) Koga, T.; Tatewaki, H.; Shimazaki, T. *Chem. Phys. Lett.* **2000**, *328*, 473.

(31) Osanai, Y.; Sekiya, M.; Noro, T.; Koga, T. *Mol. Phys.* **2003**, *101*, 65.

(32) Simon, S.; Duran, M.; Dannenberg, J. J. *J. Chem. Phys.* **1996**, *105*, 11024.

(33) Chalasinski, G.; Szczesniak, M. M. *Chem. Rev.* **2000**, *100*, 4227.

(34) Treesukol, P.; Limtrakul, J.; Truong, T. N. *J. Phys. Chem. B* **2001**, *105*, 2421.

(35) Stefanovich, E. V.; Truong, T. N. *J. Phys. Chem. B* **1998**, *102*, 3018.

(36) Jungsuttiwong, S.; Khongpracha, P.; Truong, T. N.; Limtrakul, J. *Stud. Surf. Sci. Catal.* **2001**, *135*, 2518.

(37) Jungsuttiwong, S.; Limtrakul, J.; Truong, T. N. *J. Phys. Chem. B* **2005**, *109*, 13342.

(38) Khaliullin, R. Z.; Bell, A. T.; Kazansky, V. B. *J. Phys. Chem. A* **2001**, *105*, 10454.

(39) Treesukol, P.; Kanokthip, S.; Jumras, L.; Truong, T. N. *J. Phys. Chem. B* **2005**, *109*, 11940.

(40) Frisch, M. J.; Trucks, G. W.; Schlegel, H. B.; Scuseria, G. E.; Robb, M. A.; Cheeseman, J. R.; Montgomery, Jr., J. A.; Vreven, T.; Kudin, K. N.; Burant, J. C.; Millam, J. M.; Iyengar, S. S.; Tomasi, J.; Barone, V.; Mennucci, B.; Cossi, M.; Scalmani, G.; Rega, N.; Petersson, G. A.; Nakatsuji, H.; Hada, M.; Ehara, M.; Toyota, K.; Fukuda, R.; Hasegawa, J.; Ishida, M.; Nakajima, T.; Honda, Y.; Kitao, O.; Nakai, H.; Klene, M.; Li, X.; Knox, J. E.; Hratchian, H. P.; Cross, J. B.; Bakken, V.; Adamo, C.; Jaramillo, J.; Gomperts, R.; Stratmann, R. E.; Yazyev, O.; Austin, A. J.; Cammi, R.; Pomelli, C.; Ochterski, J. W.; Ayala, P. Y.; Morokuma, K.; Voth, G. A.; Salvador, P.; Dannenberg, J. J.; Zakrzewski, V. G.; Dapprich, S.; Daniels, A. D.; Strain, M. C.; Farkas, O.; Malick, D. K.; Rabuck, A. D.; Raghavachari, K.; Foresman, J. B.; Ortiz, J. V.; Cui, Q.; Baboul, A. G.; Clifford, S.; Cioslowski, J.; Stefanov, B. B.; Liu, G.; Liashenko, A.; Piskorz, P.; Komaromi, I.; Martin, R. L.; Fox, D. J.; Keith, T.; Al-Laham, M. A.; Peng, C. Y.; Nanayakkara, A.; Challacombe, M.; Gill, P. M. W.; Johnson, B.; Chen, W.; Wong, M. W.; Gonzalez, C.; Pople, J. A. *Gaussian 03, R. C.*; Gaussian, Inc., Wallingford CT, 2004.

(41) Brock, L. R.; Duncan, M. A. *J. Chem. Phys.* **1995**, *103*, 9200.

(42) Kalus, G.; Litzén, U.; Launay, F.; Tchang-Brillet, W.-U. L. *Phys. Scr.* **2002**, *65*, 46.

(43) Bellert, D.; Breckenridge, W. H. *Chem. Rev.* **2002**, *102*, 1595.

JP902798W